J Low Temp Phys (2007) 149: 209–221
DOI 10.1007/s10909-007-9515-6

Specific Heat of ^{4}He Confined in Cylindrical Micro-Channels and Near the Superfluid Transition

Tahar Aouaroun · Guenter Ahlers

Received: 15 June 2007 / Accepted: 23 July 2007 / Published online: 9 October 2007

Abstract We present new measurements of the specific heat C_P of ^{4}He confined in cylindrical micro-channels of diameter $L = 1.89$ μm at saturated vapor pressure and near the bulk superfluid-transition temperature T_λ. The results, when combined with the specific-heat exponent $\alpha = -0.01264$, and with the correlation-length exponent $\nu = 0.6709$ obtained from α by hyper-scaling, support the departure from a universal, size independent, scaling function reported before by Lipa et al. [J. Low Temp. Phys. 124(3–4): 443, 2001] for $L = 8.17$ μm and 0.26 μm. In agreement with Lipa et al., we found that a size independent effective scaling function can be recovered within experimental resolution when an empirical effective correlation-length exponent $\tilde{\nu} = 0.716$ is used. As expected from theory, well away from T_λ the temperature dependence of the suppression of C_P by the confining medium is consistent with a power law with an exponent equal to $\alpha + \nu = 0.658$. The universal ratio of the suppression at equal distances below and above the transition was measured to be $R_{f2} = 2.3 \pm 0.2$. This result is consistent with the theoretical value $R_{f2} = 2.06$ obtained by Bhattacharyya and Bhattacharjee and is close also to the ratio $R_\xi \simeq 2.7$ of the correlation-length amplitudes.

1 Introduction

The correlation length for order-parameter fluctuations and various thermodynamic and transport properties of infinitely extended systems have singularities at critical points [1]. When the samples are confined in one physical dimension, then these singularities are modified; when the confinement is in two of the three dimension, then the phase transition no longer occurs and the properties show "rounded" temperature dependences in the vicinity of the bulk transition temperature [2, 3]. The precise,

T. Aouaroun · G. Ahlers (✉)
Department of Physics and iQCD, University of California, Santa Barbara, CA 93106, USA
e-mail: guenter@physics.ucsb.edu

quantitative, nature of this finite-size effect has been the topic of extensive theoretical and experimental study. In the present paper we contribute further to this field by presenting new measurements of the heat capacity at saturated vapor pressure C_s of liquid ^{4}He confined in cylindrical tubes near the bulk superfluid transition-temperature T_λ. It can be shown that, to a very good approximation, C_s is equal to the heat capacity at constant pressure C_P.

As seen in earlier work, we find a smooth temperature dependence of $C_P(T)$ with a maximum somewhat below T_λ. Our measurements are for helium contained in arrays of cylinders of diameter $L = 1.89$ μm that are available in "micro-channel plates", also known as "glass capillary arrays" (GCAs). We compare our results with previous measurements by others for $L = 8.17$ μm GCAs, and for 0.26 μm cylindrical pores in "Anopore". Close to the bulk transition this comparison shows departures from the theoretically expected scaling of the finite-size effect with L. In agreement with theory, far away from the bulk transition the results reveal a surface effect on C_P. The ratio of the size of this effect at equal distances above and below T_λ is within error equal to the ratio of the correlation-length amplitudes.

Confined He-4 is exceptionally suitable for the detailed experimental study of critical phenomena because, except for the effect of gravity [4, 5], the samples are homogeneous and pure [6]. It also has been the subject of many theoretical and computational investigations [7–14]. Results for C_P are often expressed in terms of the scaling function [9]

$$f_1(x) = [C_P(t, L) - C_P(t_0, \infty)](L/\xi_0)^{-\alpha/\nu}. \tag{1}$$

Here $t \equiv (T - T_\lambda)/T_\lambda$,

$$x = t(L/\xi_0)^{1/\nu}, \tag{2}$$

and $t_0 = (\xi_0/L)^{(1/\nu)}$, with $\xi_0 = 1.43 \times 10^{-10}$ m (for our sample we have $t_0 = 7.20 \times 10^{-7}$). When expressed in this form, it is expected that data for different values of L will collapse onto a unique curve for all systems that fall within a given universality class [15], i.e. in our case for ^{4}He confined in cylinders. The function f_1 is useful primarily to check the finite-size effect near the bulk transition, where the correlation length is of the order of or greater than the system size. Further away from the transition the influence of the confining geometry is primarily a surface effect, and a function more suitable for its analysis is [9]

$$f_2(x) = [C_P(t, \infty) - C_P(t, L)](L/\xi_0)^{-\alpha/\nu}. \tag{3}$$

For $x \gg 1$ it is expected that f_2 is determined by the volume of the fluid that is within a correlation length of the confining surface, leading to $f_2 = f_{20}^{\pm} x^{-(\alpha+\nu)}$ where $^+$ and $^-$ refer to the amplitude above and below T_λ respectively.

Much experimental effort has been devoted to verifying the expected scaling behavior expressed by (1) and (3) using He-4 near T_λ under various conditions of confinement [16–25]. Thanks to recent developments in fabrication techniques confining media of very well defined shapes and sizes can now be produced, and it is thus possible to compare with good confidence experimental data with theoretical expectations. In their investigation of cylindrical geometries with $L = 8.17$ μm and

0.26 μm, Lipa et al. [24] found that, contrary to expectations, the function $f_1(x)$ was size dependent. However, the difference between their two values of L was quite large, making the present measurements at an intermediate value very desirable.

2 Experimental Details

The sample cell was made of a top and a bottom OFHC copper plate that were indium-sealed together. It housed two identical micro-channel plates, one next to the other on the same horizontal plane. This configuration has the advantage over stacking one upon the other of giving more signal from the confined liquid helium without adding to the hydrostatic pressure effect. The cell design allowed some space for bulk liquid helium in the same plane as the confined sample. This bulk was needed to locate T_λ from the sharp peak which it contributed to the heat capacity. The cell was suspended from a mounting stage by two vespel supporting rods of very low thermal conductance. Above it were five stages of thermal isolation at various temperatures, the upper ones with micro-Kelvin and the lower ones with nano-Kelvin stability. Both the mounting stage and the sample stage were surrounded by a thermal shield to prevent radiation heat input. The shield was always kept within a milli-Kelvin of the cell temperature. This design ensured high thermal stability and allowed using very small temperature steps for high-resolution specific-heat measurements.

Each micro-channel plate was 1 mm thick, had a diameter of 2.48 cm, and contained an array of cylindrical micro-channels of a given diameter. The micro-channels were distributed within an active area with a diameter of about 2.0 cm. Scanning electron-microscopy showed that the channels had remarkably uniform diameters, as can be seen in Fig. 1.

The plates had a porosity of about 60%. Flow-impedance and image-analysis methods were used to evaluate the actual average diameter of the channels, which was found to be equal to 1.89 ± 0.05 μm. The amount of the sample necessary to fill the cell without overfilling was estimated from the geometrical sizes of the design, and later checked more accurately by fitting the heat-capacity data to appropriate

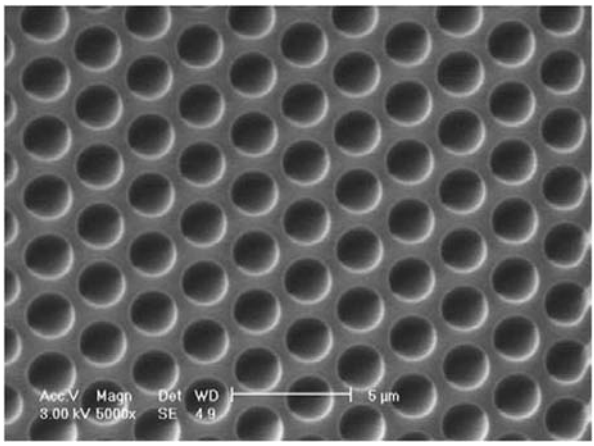

Fig. 1 Scanning electron-microscopy picture of the micro-channels of nominally 2 μm diameter. The *horizontal bar* corresponds to 5 μm

model equations as discussed below. A low-temperature helium-pressure-actuated normally-closed valve [26] was mounted on the sample chamber and sealed the sample.

Central to achieving high-resolution heat-capacity measurements was using high-resolution paramagnetic-salt thermometers (HRT) [27–29]. Initially we used a design in which the paramagnetic salt was copper ammonium bromide dihydrate $[Cu(NH_4)_2Br_4 * 2H_2O]$ (CAB) [27, 28]. It has a Curie temperature $T_c = 1.8$ K, very close to T_λ, thus allowing high resolution temperature measurements and very small temperature steps. We found that our version of these thermometers [28] lost much of their sensitivity with aging and/or thermal cycling. Thus we later changed to a new design where the paramagnet was a PdMn alloy [29]. A detailed description of the thermometer design was given by Fu et al. [28]. The HRTs were calibrated against a germanium-resistance thermometer (GRT) that in turn had been calibrated on the International Temperature Scale of 1990 (ITS-90). Such a calibration was done during each cool down. The sensitivity achieved by the thermometers was near 1 ϕ_0/μK where ϕ_0 is the quantum of magnetic flux.

To measure the specific heat, the cell temperature was allowed to drift very slowly toward that of the mounting stage. After the drift was small enough, the temperature was recorded continuously and a sequence of heat pulses was applied. Each heat pulse lasted 10 to 30 seconds and was followed by a waiting period of several minutes as needed to establish a linear drift. After many pulses, the cell was hotter than the mounting stage and the mounting-stage temperature was increased so as to bring the cell once again to an acceptable drift rate for another series of pulses. To extract the temperature change ΔT due to a heat pulse, the drifts before and after each pulse were extrapolated to the middle of the heating period. Altogether nearly 900 data points for the heat capacity were obtained, but this number was reduced to approximately 180 by averaging some adjacent points as deemed appropriate on the basis of the density of the original data.

3 Model for the Bulk Heat Capacity

A knowledge of the bulk heat capacity C_B is required for the determination of the total number of moles of sample n_0, for the number of moles n_B of bulk contributing to n_0, and for the determination of the scaling functions f_1 and f_2. The determination of n_0 and of n_B does not require extremely accurate values of C_B, but the scaling functions f_1 and especially f_2 are extremely sensitive to the precise values used to represent C_B.

Several different model equations, fitted to experimental data for C_B, have been suggested in the literature, including those of [16, 21, 24, 30] and [6]. All of them describe very well the overall shape of C_B, but small differences, of order a percent or so, exit between them. This is a significant problem especially for the determination of f_2 from (3) which involves the small difference $[C_P(t, \infty) - C_P(t, L)]$.

We adopted primarily the model suggested most recently by Lipa et al. [30] with the parameters given in the first line of their Table II, and refer to it as LNSSC. We made this choice because it is a fit to data evaluated using the ITS-90, the same

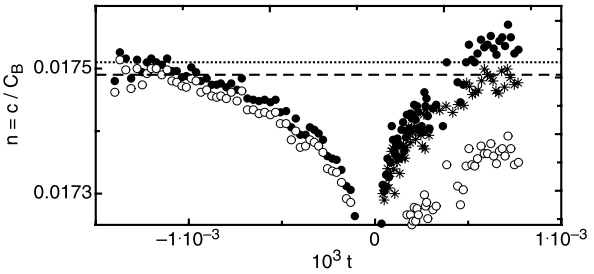

Fig. 2 The ratio $n = c/C_B$. In the absence of finite-size effects n is equal to the number of moles n_0 of liquid helium in the sample. *Solid circles*: C_B from LNSSC. *Stars*: C_B from LNSSCmod. *Open circles*: C_B from LCS. The *dotted* (*dashed*) *horizontal line* corresponds to the total number of moles $n_0 = 0.017510$ ($n_0 = 0.017495$) that we adopted on the basis of LNSSC and LNSSCmod (LCS)

temperature scale used also in the present work. There are arguments for and against this choice. On the one hand, the model, although based on extensive data below T_λ, is supported by data above T_λ that extend only up to $t \simeq 10^{-6}$. Thus the range up to our largest temperatures is essentially an extrapolation using a pure power-law fit. On the other hand, as shown by the solid circles in Fig. 2, the ratio $n = c/C_B$ of our present measurements c to the LNSSC values of C_B approaches nearly the same value at large positive and negative values of t, with a difference of perhaps 0.2%. This should be the case because finite-size effects become small and the ratio should approach n_0 on both sides of the transition. It suggests that deviations of C_B from the pure power law of LNSSC are small even as $t \to 10^{-3}$. Assuming that the model is accurate near $t = 10^{-6}$ where bulk data exist, we surmise that the interpolated model values in the range $t \leq 2 \times 10^{-4}$ which will be of interest to us should be quite reliable.

One might supplement model LNSSC, which is based on a pure power-law fit to data with $t \leq 10^{-6}$, with a confluent singularity that has a form and size determined by other measurements [6, 31] and theory [32, 33]. Various experimental data and theoretical results indicate that this singularity takes the form of a power law with an exponent of about 0.5 and an amplitude $D = \mathcal{O}(-10^{-2})$. Thus, the specific heat can be written as

$$C_B = (A/\alpha)t^{-\alpha}(1 + Dt^{0.5}) + B. \tag{4}$$

We shall refer to the model consisting of (4) with the parameters of LNSSC and $D = -0.01$ as model LNSSCmod. We find that the contribution from the confluent term is only about 0.5% of C_B at $t = 0.001$; thus a very precise value of D will not be required. The results for n computed from the data and model LNSSCmod are shown as stars in Fig. 2. They are seen to be consistent with the same value of n_0 as that found below the transition.

Finally we consider that previous evaluations [24] of (1) and (3) by Lipa et al. used a somewhat different model for C_B to which we shall refer as LCS. The difference between LCS and LNSSC approaches 1% for temperatures above T_λ as can be seen in Fig. 3. Although such a difference could perhaps be attributed to inaccuracies of LNSSC for $t \simeq 10^{-3}$ where LNSSC is not supported by data, the difference seen in

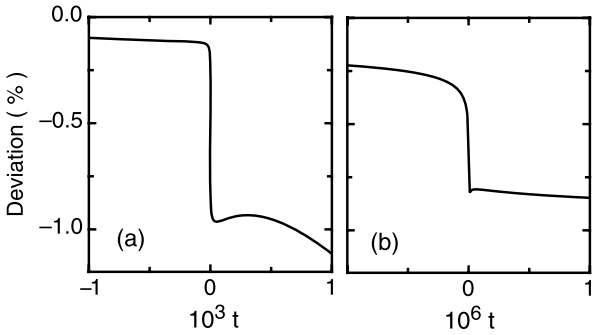

Fig. 3 The difference $100(C_{\mathrm{LNSSC}}/C_{\mathrm{LSC}} - 1)$, in percent, of the heat capacity given by LCS [24] and by LNSSC [30]. **a** and **b** give the comparison for two different temperature ranges

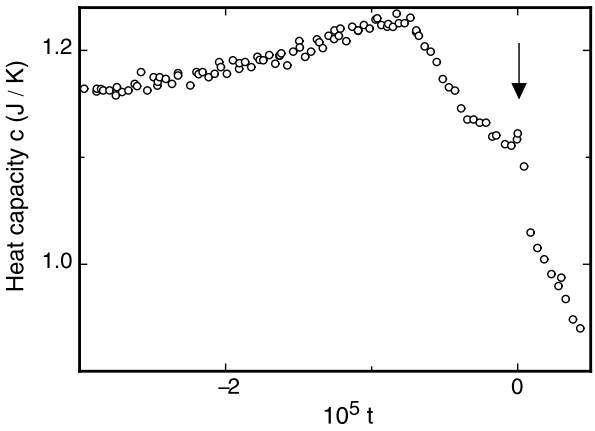

Fig. 4 Heat capacity c of the entire sample after subtraction of the heat capacity of the empty calorimeter. The *arrow* points to T_λ

the figure of about 0.8% even for $t \simeq 10^{-6}$ where LNSSC should be accurate is of some concern and can only be regarded as a measure of possible systematic errors in C_B even in these very careful heat-capacity measurements. In Fig. 2 the results for n obtained from model LCS are shown as open circles. They can not be reconciled easily with the same value of n_0 above and below the transition.

In order to obtain a sense of the influence of the model choice on the final results for f_2, we carried out parallel analyses for f_2 using LCS as well as LNSSC and LNSSCmod.

4 Data Analysis

The heat capacity of the empty cell could be represented by $c_{\mathrm{empty}} = 0.05547 + 0.1891t + 1.753t^2$ J/K. Figure 4 gives the heat capacity c of the entire helium sample (bulk and confined, before averaging) after subtracting c_{empty}, as a function of the reduced temperature t. Near the broad peak of c, c_{empty} was less than 5% of the total heat capacity. The sharp peak at $t = 0$ is a signature of the bulk transition, while the broad maximum comes from the effects of the confinement.

Although an estimate of the total number of moles n_0 of helium in the sample could be obtained from the sample volume and the filling temperature and pressure,

a better value was found by comparison of c far away from T_λ where size effects are negligible with the bulk heat-capacity per mole C_B. This was discussed already in Sect. 3, is illustrated in Fig. 2, and yielded $n_0 = 0.01751$ ($n_0 = 0.01749$) when model LNSSC or LNSSCmod (LCS) was used for $t < 0$. The measured heat capacity per mole of helium (bulk and confined) is then simply $C_{\rm tot} = c/n_0$ J/mol K. The total volume occupied by the sample, which is n_0 times the molar volume, was found to be somewhat less than the total volume of the pores in the GCA plus the bulk volume in the sample chamber.

Once the total number of moles was found, the bulk contribution had to be subtracted to get the actual contribution from the confined sample. Initially, rough estimates of confined and bulk fractions were made based on the geometrical sizes of the cell and on porosity measurements of the confining plates. The best estimate of the number of moles of bulk helium n_B, however, was determined by trying several values chosen to be close to the estimated one, and checking which one gives the smoothest variation of the specific heat

$$C_P = (c - n_B C_B)/(n_0 - n_B) \tag{5}$$

of the confined sample when passing through the bulk transition. An 18% bulk contribution, or $n_B = 0.0032$, was a good choice. The results for C_P are not very sensitive to the precise value of n_B because n_B appears both in the numerator and the denominator of (5).

In [24] (1) and (3) for f_1 and f_2, and the scaling variable x, were written in terms of L rather than L/ξ_0 leading to units involving fractional powers of length. We preferred to use the dimensionless L/ξ_0, and for comparison with our results have re-evaluated f_1, f_2, and x from the data of [22] using L/ξ_0 with $\xi_0 = 1.43 \times 10^{-10}$ m and the bulk heat capacity LNSSC or LCS.

5 Results

5.1 Qualitative Features

The finite-size specific heat obtained by subtracting the bulk contribution and dividing by the number of moles of confined helium is shown in Fig. 5. For comparison we also show data obtained by Kimball et al. for the case of micro-channels of square cross section of size 1 μm × 1 μm [25], and the data obtained by Lipa et al. for 0.26 μm diameter Anopore cylinders and 8.17 μm diameter GCA cylinders [24]. The overall shape and behavior of the data follow expected trends with the size of the confining medium.

5.2 Breakdown of Scaling Close to T_λ

Of primary interest here is the temperature range near the maximum of c, which is below T_λ. Thus, for this analysis it does not matter much whether model LCS or LNSSC is used because there the two models agree with each other (see Fig. 3). We carried

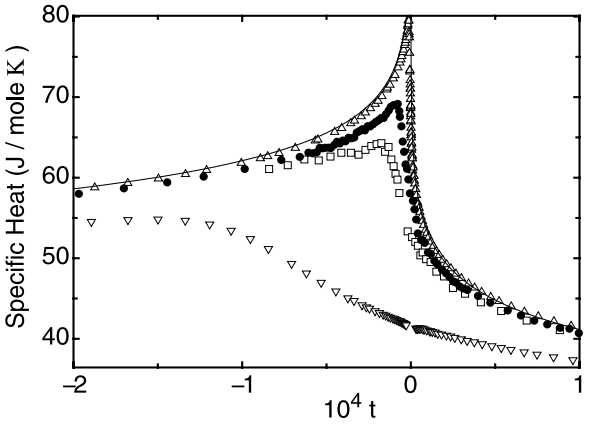

Fig. 5 Specific heat of confined helium. From *top* to *bottom*: bulk helium [30] (*solid line*, LNSSC); 8.17 μm diameter GCA cylinders [24] (*up-pointing triangles*); the present data for 1.89 μm diameter cylinders (*solid circles*, some *adjacent points* were averaged for clarity of presentation); tubes of square cross section of 1 μm × 1 μm [25] (*open squares*); 0.26 μm diameter Anopore cylinders [24] (*down-pointing triangles*)

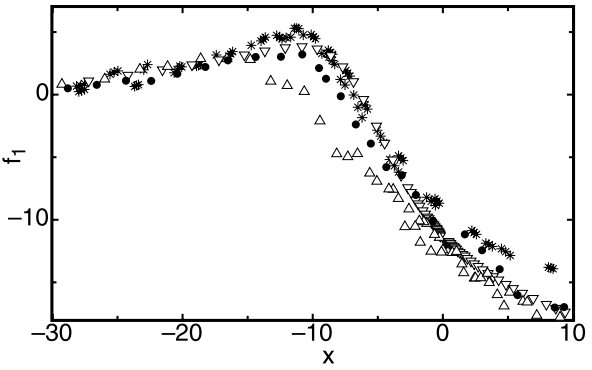

Fig. 6 Scaling function f_1 defined by (1). *Up-pointing triangles*: Lipa et al. [24], $L = 8.17$ μm; *circles*: this work, Ł = 1.89 μm). *Down-pointing triangles*: Lipa et al. [24], $L = 0.26$ μm. *Stars*: Monte Carlo calculations [13]

out the analysis using LNSSC. Finite-size scaling can be tested quantitatively by plotting the function f_1 given by (1) for various confinement sizes; if finite-size scaling is valid, then f_1 should be independent of size. To compute this function we used the bulk value $C(t_0, \infty)$ at the reduced temperature $t_0 = (\xi_0/L)^{1/\nu} = 7.20 \times 10^{-7}$ above T_λ where the correlation length is equal to the confining size. We also used [30] $\alpha = -0.01264$, and the corresponding $\nu = 0.6709$ computed from the hyper-scaling relationship $\nu = (2 - \alpha)/3$. Note that this value of ν is very close to 0.6705 which was found experimentally from superfluid-density measurements based on second-sound velocity determinations [34, 35]. In Fig. 6 we show f_1 for our data as solid circles, along with f_1 for the data of Lipa et al. [24] (triangles) and the Monte Carlo calculations by Schultka and Manousakis [13] (stars). From this latter reference, we chose the results obtained for a bar geometry with staggered boundary conditions at the walls and periodic boundary conditions along the length. This case comes closest to, but is not identical to, real experimental geometries. It is gratifying that f_1 for this case has a shape generally similar to the experimental shapes. Near the maximum of f_1, our data lie between the results for 0.26 μm and 8.17 μm, confirming a trend of f_1 with size even though f_1 was expected to be universal, i.e. size independent, if finite-size scaling were valid. The origin of departures from finite-size scaling is not yet elucidated for the case of helium. However, it is interesting to note that Chen

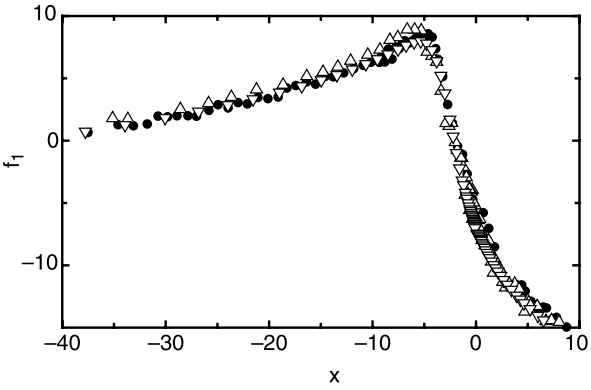

Fig. 7 The scaling function f_1 as defined by (1), but computed using the effective value $\tilde{\nu} = 0.716$ (all other parameters were kept the same). The symbols are as in Fig. 6

and Dohm [36] predicted a breakdown for certain theoretical models. From the experiment it is clear that f_1 computed from the measurements and using the accepted values of the universal exponents α and ν does not yield the expected universal behavior. A deviation from finite-size scaling of f_1 near its maximum does not seem to be specific to the cylindrical geometry; similar behavior was found also in planar geometries [23].

It was noted by Lipa et al. [24] that the dependence of the reduced temperature t_m at the maximum of C_P upon L could be fitted by a power law with an *effective* exponent $\tilde{\nu} = 0.716$. To further explore this idea, we show in Fig. 7 the results for f_1 computed with $\tilde{\nu} = 0.716$ instead of ν as in Fig. 6, keeping all other parameters the same. One sees that using $\tilde{\nu}$ to a good approximation collapses all the data onto a single curve.

5.3 The Surface-Dominated Region Further Away from T_λ

In the range further from T_λ, where finite-size or surface effects are small, the choice of the model for C_B has significant influence for $t > 0$ where LNSSC and LCS differ by about 1%. For $t < 0$ both models give nearly the same result because they agree with each other within about 0.1%. In Fig. 8a we show the scaling function f_2 defined by (3) based on model LNSSC as circles. For $t > 0$ (solid circles for LNSSC) the results from the analysis using LNSSCmod are given by stars. The equivalent results for the analysis using model LCS are given in Fig. 8b. For sufficiently large x f_2 is expected to be proportional to $x^{-(\alpha+\nu)}$ with x given by (2) [9]. Thus the data above and below T_λ are expected to fall on parallel straight lines in the figures. This expectation is fulfilled extremely well for LNSSCmod, and quite well also for LNSSC, as shown in Fig. 8a. It is not fulfilled by the data based on LCS in Fig. 8b. The deviations of LNSSC from the true specific heat may be responsible for the slight downturn in Fig. 8a of the solid circles for $x > 200$. The results based on LNSSCmod (stars) do not turn down and follow a power law up to the largest value of x that is shown. As an illustrative example of the extreme sensitivity of the analysis to small differences in the model for C_B we note that $C_P/C_B \simeq 0.99$ for $x \simeq 400$ ($t = 2.9 \times 10^{-4}$).

In a more quantitative analysis we shall focus only on the data based on LNSSC and LNSSCmod because above T_λ those based on LCS do not follow a simple power

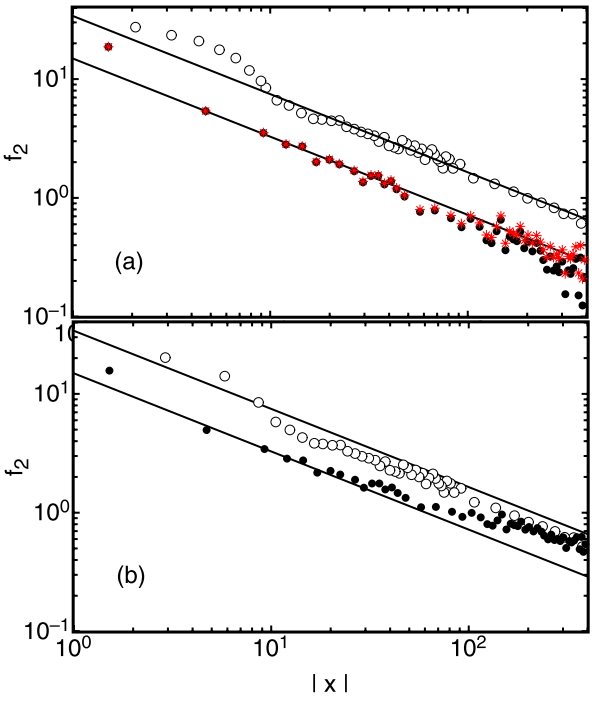

Fig. 8 (Color online) The scaling function f_2 as defined by (3), computed using **a**: LNSSC and **b**: LCS for the bulk heat capacity. *Open symbols*: $T < T_\lambda$. *Solid symbols*: $T > T_\lambda$. The *solid lines* are limited-range fits of a power law with the exponent fixed at 0.6709 to the data in **a**

law (see Fig. 8b). Using only data over the range $4 < x < 240$, a least-squares fit yielded $\alpha + \nu = 0.685 \pm 0.03$ from the data based on LNSSC. Using data for $4 < x < 400$ based on LNSSCmod, we obtained $\alpha + \nu = 0.676 \pm 0.02$. Both are consistent with the predicted value $\alpha + \nu = 0.658$. Below T_λ the results at small $|x|$ are influenced more strongly by finite-size rather than surface effects, and a power law with exponent equal to $\alpha + \nu$ would not be expected except for somewhat larger values of $|x|$. A fit over the range $40 < |x| < 400$ yielded $\alpha + \nu = 0.674 \pm 0.04$, again consistent with the expected value. The lines drawn through the data in Fig. 8 are power-law fits with the exponent fixed at $\alpha + \nu = 0.658$. These fits yielded amplitudes $f_{20}^- = 34.0 \pm 0.6$ and $f_{20}^+ = 14.9 \pm 0.3$ below and above T_λ respectively, corresponding to the universal ratio $R_{f2} \equiv f_{20}^-/f_{20}^+ = 2.3 \pm 0.1$. Here the cited uncertainty corresponds only to the random errors arising from the scatter in the data. In addition systematic errors due to possible deviation of $f_2^\pm$ at small x from a pure power law, as well as due to differences between the bulk models and the true C_B at large x, may lead to an additional uncertainty for R_{f2} that is difficult to determine but that may be in the vicinity of 0.1. Thus we cite $R_{f2} = 2.3 \pm 0.2$ as our best estimate.

The function f_2^+ above T_λ was calculated by Schmolke et al. [9] and by Mohr and Dohm [8]. Their results are generally consistent with our measurements, but for $x < \mathcal{O}(10^2)$ the prediction of [9] shows negative deviations from the power law with exponent $\alpha + \nu$. The measurements do not show these deviations. Theoretical results for R_{f2} are still only approximate. Our result is consistent with an estimate by Bhattacharyya and Bhattacharjee [37] which gave 2.06. Another calculation, by Mohr and Dohm [8], is considered by those authors to be reliable only above T_λ and

thus does not give a meaningful value of R_{f2}. We note that our measurement also agrees fairly well with an estimate of the ratio of the correlation-length amplitudes $R_\xi = \xi_0^-/\xi_0^+ \simeq 2.7$ by Hohenberg et al. [38].

The present result for R_{f2} differs significantly from the experimental results given by Lipa et al. [24] who cite the ratios 1.29 for their 8 μm GCA sample and 1.42 for their 0.26 μm Anopore sample. We believe that the origin of that difference is to be found in part in the bulk heat capacity model LCS used in the evaluation of f_2. Our result for R_{f2} also differs from that obtained by Kimball et al. [25], who gave $R_{f2} = (8.6 \pm 0.5)/(5.9 \pm 0.2) \simeq 1.4 \pm 0.2$, and from that of the micro-gravity experiment CHeX [39] which yielded a value close to 1.4. We are not aware of the origin of these differences. For further discussions of previous experiments we refer to a recent review article [40].

Our analysis illustrated the extreme sensitivity of f_2 in the range $|x| > 10^2$ to the values used for C_B in its evaluation. Given this sensitivity, one might view with caution the interpretation by others [25] of results for f_2 in terms of "surface" and "edge" contributions at values of x well above 10^3.

6 Summary

In conclusion, our results near the bulk transition support the size dependence of the finite-size scaling-function f_1 seen in previous work [24]. This departure from finite-size scaling does not seem to be specific to the cylindrical shape of the confining geometry. It appears to be a broader phenomenon as it has been seen also for planar geometries [23]. The recovery of an effective scaling, using an effective parameter $\tilde{\nu}$ instead of ν, suggests that this phenomenon can be described to a good approximation by a single, albeit as yet empirical, parameter.

Further away from the transition results are extremely sensitive to the bulk specific heat C_B with which the finite-size specific heat C_P is compared. This is illustrated by the fact that the scaling function f_2 reaches values as small as 0.7 (0.16) when the scale parameter x has a value of 10^2 (10^3). For our capillary diameter, this occurs at $t \simeq 7 \times 10^{-5}$ (7×10^{-4}) where $C_B \simeq 42$ (31) J/mol K. With $(L/\xi_0)^{-\alpha/\nu} \simeq 1.2$ one readily sees from (3) that $(1 - C_P/C_B) \simeq 0.014$ (0.004) when $x = 10^2$ (10^3). Thus a 10% measurement of f_2 requires that C_B and C_P are "consistent" with each other to within 0.14 (0.04)% at that x-value. Compared to this we saw in Fig. 3 that the two major model functions for C_B differed from each other by as much as about 1%. The message seems clear to us. A meaningful computation of f_2 in the range $x > \mathcal{O}(10^2)$ is possible only when a model is chosen that asymptotically approaches the measured C_P as $|x|$ becomes large enough so that the bulk and finite-size measurements should agree. As illustrated by Fig. 2, in our case model LNSSCmod satisfies this criterion very well, and LNSSC comes close too; but LCS does not pass this test. In this connection we emphasize that we can not know whether the "fault" for the problem with LCS is to be found in our data or with LCS. Figure 3 as well as a comparison with several other high-precision measurements of C_B show that even these vary careful experiments may yield results that differ from each other by something of order 1%. This is why above we urged "consistency" rather than accuracy (which seems to be quite unachievable at the required level).

Using the model that seems most nearly consistent with our data, namely LNSSC-mod or LNSSC, our results for the scaling function f_2 agree with the prediction that a surface contribution dominates for large $|x|$, leading to a power-law dependence of f_2 that is consistent with the exponent $\alpha + \nu = 0.658$ that was obtained from measurements on bulk helium. The ratio of the amplitude of f_2 below to that above T_λ is found to be $R_{f2} = 2.3 \pm 0.2$, which agrees well with the theoretical result $R_{f2} = 2.06$ obtained by Bhattacharyya and Bhattacharjee [37] and is close to an estimate of the ratio of the correlation-length amplitudes [38] $\xi_0^- / \xi_0^+ \simeq 2.7$. However, it differs from several previous experiments [24, 25, 39] that yielded values near 1.4. We sense that some of the previous results that differed from ours may have been influenced by "inconsistent" models for the bulk specific heat.

Acknowledgements We thank J. Lipa for numerical data corresponding to [24], and S. Manousakis for numerical values for the Monte Carlo results. This work was supported by NASA grants NAG3-2872 and NAG3-2903.

References

1. H.E. Stanley, *Introduction to Phase Transitions and Critical Phenomena* (Oxford University Press, Oxford, 1971)
2. V. Privman, in *Finite Size Scaling and Numerical Simulations of Statistical Systems*, ed. by V. Privman (World Scientific, New Jersey, 1990)
3. M.N. Barber, in *Phase Transitions and Critical Phenomena*, vol. 8, ed. by C. Domb, J.L. Lebivitz (Academic Press, New York, 1983)
4. G. Ahlers, Phys. Rev. **171**, 275 (1968)
5. G. Ahlers, J. Low Temp. Phys. **84**, 173 (1991)
6. G. Ahlers, in *The Physics of Liquid and Solid Helium, Part I*, ed. by K.H. Bennemann, J.B. Ketterson (Wiley, New York, 1976)
7. V. Dohm, Phys. Scr. T **49**, 46 (1993)
8. U. Mohr, V. Dohm, Physica B **284–288**, 43 (2000)
9. R. Schmolke, A. Wacker, V. Dohm, D. Frank, Physica B **165–166**, 575 (1990)
10. A. Wacker, V. Dohm, Physica B **194–196**, 611 (1994)
11. N. Shultka, E. Manousakis, Phys. Rev. Lett. **75**, 2710 (1995)
12. N. Shultka, E. Manousakis, J. Low Temp. Phys. **109**(5–6), 733 (1997)
13. N. Shultka, E. Manousakis, J. Low Temp. Phys. **111**(5–6), 783 (1998)
14. K. Nho, E. Manousakis, Phys. Rev. B **68**, 174503 (2003)
15. M.E. Fisher, Rev. Mod. Phys **70**, 653 (1998)
16. T. Chen, F. Gasparini, Phys. Rev. Lett. **40**, 410 (1978)
17. I. Rhee, F. Gasparini, Phys. Rev. Lett. **63**, 410 (1989)
18. J.A. Nissen, T.C.P. Chui, J.A. Lipa, J. Low Temp. Phys. **92**(5–6), 783 (1993)
19. M. Coleman, J.A. Lipa, Phys. Rev. Lett. **74**, 286 (1995)
20. S. Mehta, F. Gasparini, Phys. Rev. Lett. **78**, 2596 (1997)
21. S. Mehta, M. Kimball, F. Gasparini, J. Low Temp. Phys. **114**(5–6), 467 (1999)
22. J.A. Lipa, D.R. Swanson, J.A. Nissen, Z.K. Geng, P.R. Williamson, D.A. Stricker, T.C.P. Chui, U.E. Israelsson, M. Larson, Phys. Rev. Lett. **84**, 4894 (2000)
23. M. Kimball, S. Mehta, F. Gasparini, J. Low Temp. Phys. **121**(1/2), 29 (2000)
24. J.A. Lipa, M. Coleman, D.A. Stricker, J. Low Temp. Phys. **124**(3–4), 443 (2001)
25. M.O. Kimball, K.P. Mooney, F.M. Gasparini, Phys. Rev. Lett. **92**, 115301 (2004)
26. V. Dotsenko, N. Mulders, J. Low Temp. Phys. **134**(1–2), 443 (2004)
27. T.C.P. Chui, D.R. Swanson, M.J. Adriaans, J.A. Nissen, J.A. Lipa, Phys. Rev. Lett. **69**, 3005 (1992), and Ref. [6] therein
28. H. Fu, H. Baddar, K. Kuehn, M. Larson, N. Mulders, A. Schegolev, G. Ahlers, J. Low Temp. Phys. **111**(1–2), 49 (1998)

29. B.J. Klemme, M.J. Adriaans, P.K. Day, D.A. Sergatskov, T.L. Aselage, R.V. Duncan, J. Low Temp. Phys. **116**, 133 (1999)
30. J.A. Lipa, J.A. Nissen, D.A. Stricker, D.R. Swanson, T.C.P. Chui, Phys. Rev. B **68**, 174518 (2003)
31. D.S. Greywall, G. Ahlers, Phys. Rev. Lett. **28**, 1251 (1972)
32. F.J. Wegner, Phys. Rev. B **5**, 4529 (1972)
33. A. Aharony, G. Ahlers, Phys. Rev. Lett. **44**, 782 (1980)
34. L.S. Goldner, G. Ahlers, Phys. Rev. B **45**, 13129 (1992)
35. L.S. Goldner, N. Mulders, G. Ahlers, J. Low Temp. Phys. **93**, 125 (1993)
36. X.S. Chen, V. Dohm, Eur. Phys. J. B **10**, 687 (1999)
37. S. Bhattacharyya, J.K. Bhattacharjee, Phys. Rev. B **61**, 5899 (2000)
38. P.C. Hohenberg, A. Aharony, B.J. Halperin, E.D. Siggia, Phys. Rev. B **13**, 2986 (1976)
39. J.A. Lipa, D.R. Swanson, J.A. Nissen, Z.K. Geng, P.R. Williamson, D.A. Stricker, T.C.P. Chui, U.E. Israelsson, M. Larson, Phys. Rev. Lett. **84**, 4894 (2000)
40. M. Barmatz, I. Hahn, J.A. Lipa, R.V. Duncan, Rev. Mod. Phys. **79**, 1 (2007)